

Mapping the Galactic Halo IV. Searching for Distant Giants with the Washington System

Heather L. Morrison^{1,2}

Department of Astronomy, Case Western Reserve University, Cleveland OH 44106-7215
electronic mail: heather@vegemite.astr.cwru.edu

Edward W. Olszewski

Steward Observatory, University of Arizona, Tucson, Arizona 85726
electronic mail: edo@as.arizona.edu

Mario Mateo

Department of Astronomy, University of Michigan, 821 Dennison Bldg., Ann Arbor, MI
48109-1090
electronic mail: mateo@astro.lsa.umich.edu

John E. Norris

Mount Stromlo and Siding Spring Observatories, ANU, Private Bag, Weston Creek PO, 2611
Canberra, ACT, Australia
electronic mail: jen@mso.anu.edu.au

Paul Harding

Steward Observatory, University of Arizona, Tucson, Arizona 85726
electronic mail: harding@billabong.astr.cwru.edu

R.C. Dohm-Palmer³

Department of Astronomy, University of Michigan, 821 Dennison Bldg., Ann Arbor, MI
48109-1090
electronic mail: rdpalmer@astro.lsa.umich.edu

Kenneth C. Freeman

Mount Stromlo and Siding Spring Observatories, ANU, Private Bag, Weston Creek PO, 2611
Canberra, ACT, Australia
electronic mail: kcf@mso.anu.edu.au

¹Cottrell Scholar of Research Corporation and NSF CAREER fellow

²and Department of Physics

ABSTRACT

We critically examine the use of the Washington photometric system (with the 51 filter) for identifying distant halo giants. While this is the most powerful photometric technique for isolating G and K giant stars, spectroscopic follow-up of giant candidates is vital. There are two situations in which interlopers outnumber genuine giants in the diagnostic $M-51/M-T_2$ plot, and are indistinguishable photometrically from the giants. (1) In deep surveys covering tens of square degrees, very metal-poor halo dwarfs are a significant contaminant. An example is our survey of the outer halo (Morrison et al. 2000a; Dohm-Palmer et al. 2000), where these metal-poor dwarfs dominate the number of photometric giant candidates at magnitudes fainter than $V = 18$ and cannot be isolated photometrically. (2) In deep surveys of smaller areas with low photometric precision, most objects in the giant region of the color-color plot are dwarfs whose photometric errors have moved them there. Color errors in $M-51$ and $M-T_2$ need to be smaller than 0.03 mag to avoid this problem. An example of a survey whose photometric errors place the giant identifications under question is the survey for extra-tidal giants around the Carina dwarf spheroidal of Majewski et al. (2000a). Accurate photometry and spectroscopic follow-up of giant candidates are essential when using the Washington system to identify the rare outer-halo giants.

Subject headings:

1. Introduction

Photometric searches over wide areas for rare, distant giants in the Galactic halo are now a reality, thanks to the advent of wide-field CCD systems. One particularly useful photometric system is the Washington system (Canterna 1976; Harris and Canterna 1979). Since Geisler (1984) added the DDO “51” filter to allow discrimination between late-type dwarfs and giants and re-calibrated its [Fe/H] indicator, this system has steadily gained in popularity. Its broad-band filters and strong abundance sensitivity for late-type giants (Geisler et al. 1991; Paltoglou and Bell 1994) mean that it was well-suited to studies of objects of known distance such as open and globular cluster giants. In these cases there is little need for luminosity discrimination.

However, when seeking rare objects such as halo giants, which are seen through a thick veil of foreground disk stars, luminosity discrimination is vital. The Mg b /MgH feature near 5170Å is strong in late-type dwarfs and weak in giants. The “51” filter (with $\lambda_c = 5130\text{\AA}$ and $\Delta\lambda = 154\text{\AA}$) is centered on this feature. It works well for discriminating between late G/K dwarfs of

³Postdoctoral Research Scientist, Steward Observatory

solar or near-solar metallicity and G/K giants. The addition of this filter has allowed the use of the Washington system in surveys for late G and K giants where foreground contamination by disk dwarfs is a problem. This is superior to other photometric methods of identifying giants such as DDO or Strömgren photometry (McClure and Forrester 1981; Bond 1980) because only one filter has a narrow passband, and it is not necessary to observe in the ultraviolet. Surveys well-suited to the Washington system include:

- studies of giant stars in clusters at low latitude, where it is now possible to remove foreground dwarf non-members (eg Geisler, Claria and Minniti 1997)
- surveys for rare field giants of the outer halo (Morrison et al. 2000a, Paper I hereafter; Majewski et al. 2000b)
- surveys for extra-tidal giants from Galactic dwarf satellites (Majewski et al. 1999, 2000a)

The last two types of survey make contributions to our understanding of the formation and subsequent evolution of the Galaxy. Distant halo field giants, such as the one recently discovered by our survey at 90 kpc (Olszewski et al. 2000) provide in-situ probes of the outer halo, and are also important probes of the Galactic potential (Zaritsky et al. 1989). But their identification as giants must be solid in order to make them useful – the spatial distribution and kinematics of local halo dwarfs will contribute little to our understanding of the outer Galaxy. Indeed, misidentification will lead to serious errors.

We began work on this paper in order to understand our low success rate at identifying halo giants for V magnitudes fainter than 18. For brighter magnitudes our success rate, confirmed by spectroscopic follow-up, is better than 90%, but this falls precipitously to 24% for V magnitudes between 18 and 19 (Dohm-Palmer et al. 2000), despite comparably good mean photometric uncertainties for these fainter stars.

A detailed investigation into the limitations of the Washington luminosity classification may also cast light on some surprising claims from the surveys around dwarf satellites of the Milky Way. For example, Majewski et al. (2000a) have claimed detection of large numbers of extra-tidal stars in the Carina dwarf spheroidal galaxy. Such a large extra-tidal population, if confirmed, has implications not only for galaxy evolution but also for our understanding of the dark matter content of the dSph satellites. However, these surveys extend to much fainter magnitudes than previously possible, and it is important to understand possible contamination by foreground and background objects, and the role of photometric errors, at such faint levels.

Our essential result is that there are two major problems with the Washington luminosity classification: first, very metal-poor foreground subdwarfs are indistinguishable photometrically from halo giants; second, photometric errors can scatter disk dwarfs into the halo giant region of the $M-T_2/M-51$ diagnostic plot.

In Section 2 we discuss possible contaminants of halo giant candidates in the $M-T_2/M-51$ diagram: disk and halo dwarfs, galaxies and QSOs. With accurate $M-51$ photometry, the only serious contaminants are the very metal-poor halo dwarfs whose weak lines make them indistinguishable photometrically from halo giants. We derive a luminosity function specifically for such metal-poor halo dwarfs and use it, with a simple halo model, to predict the number of subdwarfs per deg² in different directions in the Galaxy.

Although foreground disk and thick disk dwarfs are negligible contaminants if accurate photometry is obtained, the high density of these stars, especially at low latitudes, makes the number scattered into the giant region of the $M-T_2/M-51$ diagram a sensitive function of photometric error. In Section 3 we investigate this in detail, and describe the double effect of large errors on giant searches: not only are dwarfs scattered into the giant region, but genuine giants are scattered out.

In Section 4 we use what we have learned about giant selection to examine our own pencil-beam survey of at high galactic latitudes (Dohm-Palmer et al. 2000). The BTC subset (obtained using the Big Throughput Camera on the CTIO 4m in April 1999) covers 12.7 square degrees, and has spectroscopic follow-up of approximately half of the giant candidates (Morrison et al. 2000b). We find that foreground subdwarfs are the principal cause of our low detection efficiency for giants below $V = 18$, and describe our plans to optimize future searches for the faint, red giants of the extreme outer halo so that fewer subdwarfs are misidentified as giants.

In Section 5 we discuss the survey of Majewski et al. (2000a) (MOPKJG hereafter) of approximately two square degrees centered on the Carina dwarf spheroidal galaxy. Their study found a large number (~ 100) of giant candidates outside the tidal radius of Irwin and Hatzidimitriou (1995), but they were only able to obtain follow-up spectra of three of the brightest extra-tidal candidates. The photometric errors of the MOPKJG data are more typical of photographic than of CCD photometry, and we discuss the possible effect of these errors on the giant selection.

2. Use of the 51 Filter – Disk Dwarfs and Other Problems

2.1. Foreground Disk Dwarfs

Geisler (1984) showed the sensitivity of the $M-51$ index to luminosity for late G and K stars, and this was confirmed and expanded by Paltoglou and Bell (1994) using synthetic spectra. The index loses sensitivity to luminosity blueward of $M-T_2 = 1.1$. It holds almost no luminosity information blueward of $M-T_2 = 1.0$, due to the disappearance of the MgH feature in dwarfs at this temperature. This can be seen clearly in Figure 7 of Paltoglou and Bell (1994) for $T_1 - T_2 < 0.4$ ($M-T_2 < 1.0$).

The $M-51$ index works well for discrimination between halo giants and foreground dwarfs of the thin and thick disk (mean [Fe/H] of -0.2 and -0.5, McWilliam (1990); Carney, Latham and

Laird (1989)). The separation between the $[\text{Fe}/\text{H}] = -0.5$ dwarf and the $[\text{Fe}/\text{H}] = -1.0$ giant lines ranges from 0.075 to 0.23 mags at $M-T_2 = 1.1$ and 1.8, respectively. Only large photometric errors (explored further in Section 3 below) will cause thin or thick disk dwarfs to appear in the giant region. We define our giant selection region as that bounded by $M-T_2 = 1.1$ (where the index loses sensitivity) and 1.8 (where the Washington abundance calibration stops) and $M-51 = -0.02$ and 0.09, but excluding the area below the line between $(M-T_2, M-51) = (1.1, 0.02)$ and $(1.2, -0.02)$. (The giant selection region is illustrated below in Figures 4 and 15).

2.2. Foreground Subdwarfs

As we noted in Paper I, metal-poor dwarfs of $[\text{Fe}/\text{H}] \leq -2.0$ overlap the giant region in the $M-51$ vs. $M-T_2$ diagram, and follow-up spectroscopy is needed to weed them from the sample. Few bright examples of such stars are known, due to their intrinsic rarity and low luminosity, and at the time of writing Paper I we had only obtained spectra of one such star, G30-52, $[\text{Fe}/\text{H}] = -2.06$, (Carney et al. 2000), which lies at the extreme blue end of our selection region. Since then we have obtained spectra of several more very metal-poor K dwarfs, which are shown in Figure 1. All but the most weak-lined star, G160-30, have metallicity determinations from high-dispersion spectroscopy, whose sources are given in Table 1.

We have made an initial estimate⁴ from our low resolution spectra and find the metallicity of G160-30 to be $[\text{Fe}/\text{H}] = -3.0$. This star is particularly useful for calibrating our survey because of its relatively cool temperature ($(B-V)_0 = 1.0$, using the reddening estimates of Schlegel et al. (1998) and the photometry of Carney et al. (2000)). At first sight it is difficult to distinguish between the spectra of G160-30 and that of a very metal-poor giant such as NGC 5053-D (see Figure 3 of Paper I). We will discuss this further in Morrison et al. (2000b), where we will show that the ratio of strengths of neutral and ionized Ca lines discriminates between such giants and dwarfs in spectra of sufficient S/N.

In Paper I we made an estimate of the number of subdwarfs with $[\text{Fe}/\text{H}]$ less than -2.0 in our survey’s magnitude range using the Bahcall-Soniera model (Bahcall and Soniera 1984) scaled by the proportion of halo stars with $[\text{Fe}/\text{H}] < -2.0$. In the Appendix we derive a luminosity function (LF) specifically for the halo subdwarfs which appear in our giant selection region. Since the determination of the halo field LF of Bahcall and Casertano (1986) only contains 51 stars over all abundances in the absolute magnitude range of interest, we cannot derive an accurate LF from the metal-poor subset of the Bahcall and Casertano (1986) data. Thus we choose to use accurate LFs constructed from HST observations of four very metal-poor globular clusters, and use the HST color-magnitude diagram of NGC 6397 King et al. (1998) to transform from M_V to $V-I$ and hence $M-T_2$. Details are given in the Appendix.

⁴using synthetic spectra computed by one of us (JEN)

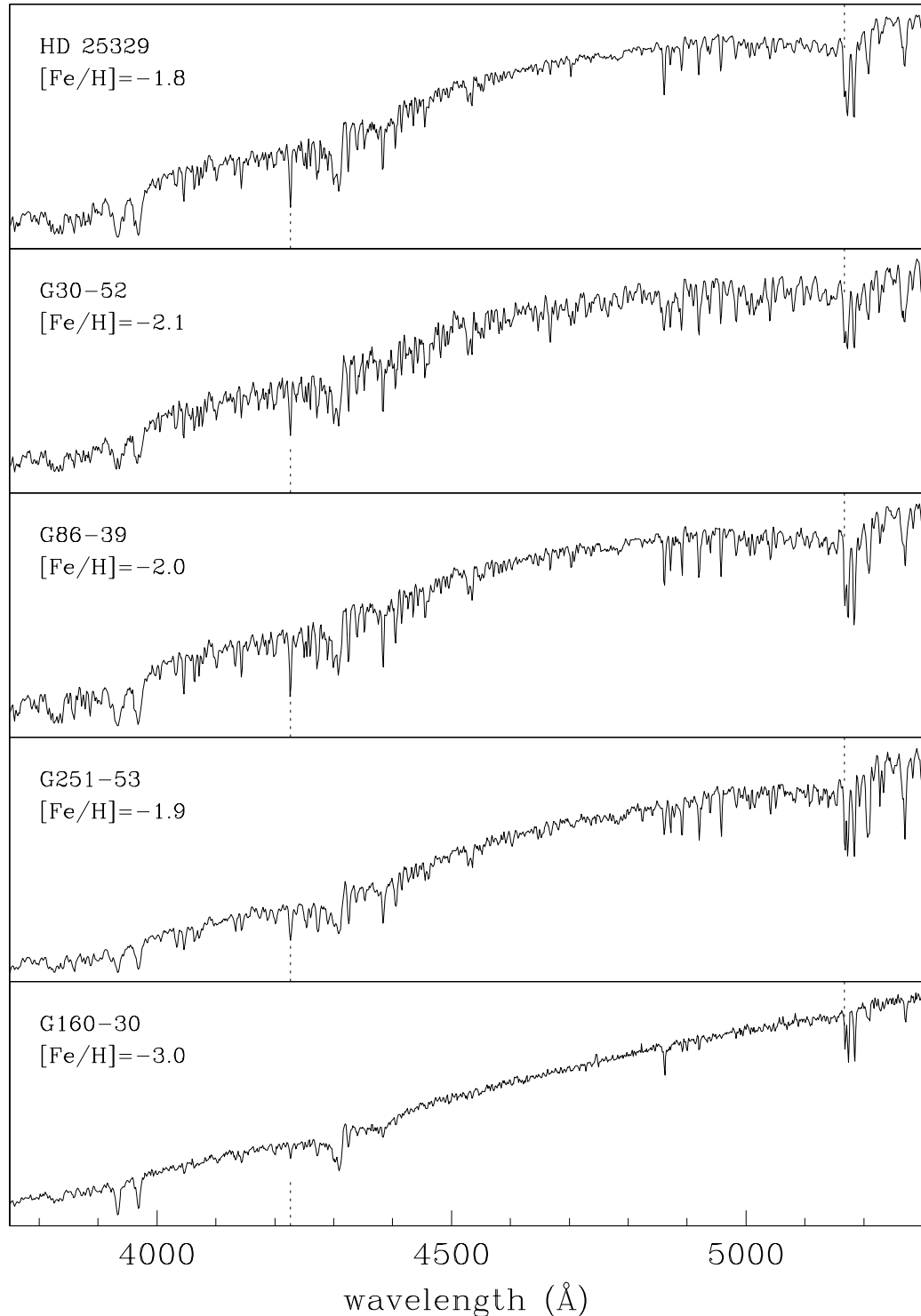


Fig. 1.— Spectra of known subdwarfs in our giant color range with $[\text{Fe}/\text{H}]$ less than -1.7 . Positions of the CaI 4227 \AA line and the Mg line at 5167 \AA are marked.

How distant will these contaminating subdwarfs be? Using the deep $V, V - I$ color-magnitude diagram of NGC 6397 of King et al. (1998), transformed to the standard Landolt system following Holtzman et al. (1995) and a distance modulus of $(m - M)_V = 12.36$, we find that $M - T_2 = 1.2$ corresponds to $M_V = 7.1$. In a survey such as ours, currently limited to $V < 19$ by spectroscopic follow-up, this corresponds to distances up to 2.5 kpc from the Sun.

Our halo dwarf model assumes the luminosity function given in the Appendix in Table 3. The halo’s spatial distribution is modelled using a power-law exponent of -3.0 and a moderate flattening of $b/a = 0.6$ — values confirmed by halo turnoff stars found in our survey (Morrison et al. 2000a). Figure 2 shows its predictions for our giant selection box. The number of subdwarfs is a strong function of magnitude, reaching tens per deg 2 for $V \sim 20$.

2.3. Binary Stars

Since up to 50% of all stars may be binaries, it is worth considering whether two stars in a binary system can masquerade as a single giant. This is trivially true of a binary system consisting of a giant and a faint dwarf companion, since the giant luminosity will dominate. However, it is a little less clear whether a binary system composed of two main sequence stars could have $M - T_2$ and $M - 51$ colors within the giant region.

To test this we took the synthetic $M - T_2$ and $M - 51$ colors of Paltoglou and Bell (1994) and of Bessell (2000) for stars with T_{eff} ranging from 4000 to 10000 K, $log g$ from 4.5 to 0.7, and [Fe/H] from 0 to -1.0 , and combined them into simulated binary systems using the absolute magnitudes given in Bessell (2000). Since Paltoglou and Bell (1994) only give colors for stars from 4000 to 7000 K, and Bessell (2000) does not give $M - 51$ colors, we set the $M - 51$ color of all stars hotter than 7000 K at 0.017, which is the color expected for a spectrum with no features in the Mg b/MgH region. The only stars for which the binary system had both $M - T_2$ and $M - 51$ in our giant region were those for which one component of the binary system already had colors within the giant region. This is because (1) the bluer component of a binary made of two main sequence stars will be brighter and so dominate the $M - T_2$ color, and (2) it is not possible in a spectrum without emission lines to have $M - 51$ significantly higher than 0.017 unless one star is extremely metal-poor.

Thus contamination by binary stars whose constituent stars are both on the main sequence is negligible.

2.4. Galaxies and QSOs

Because of the emission lines and redshifted features in galaxy and QSO spectra, they can be found both in the giant region of the $M - 51/M - T_2$ plot, and also in regions not occupied by normal stars. The synthetic $M - 51$ colors of Paltoglou and Bell (1994) for very metal-poor stars

Table 1. Metallicity and color of stars in Fig. 1

Star ID	[Fe/H]	$(b-y)_0$	$(V-I)_0$	$(B-V)_0$	$(M-T_2)_0$	$E(B-V)$	Source
HD 25329	-1.76	0.529	1.10	0.04	2,3,7,8,9
G30-52	-2.1	0.498	1.10	0.00	1,2,5
G86-39	-2.0	0.522	1.20	0.00	1,2,3
G160-30	-3.0	1.00	1.50	0.11	2,5
G251-53	-1.87	...	1.24	...	1.57	0.00	2,3,4,6

Note. — 1: Carbon, et al. (1987); 2: Carney et al. (2000); 3: Alonso, Arribas and Martinez-Roger (1996); 4: Ryan (1992); 5: Schlegel et al. (1998); 6: Ivans et al. (2000) 7: Beveridge and Sneden (1994); 8: Tomkin and Lambert (1999); 9: Gratton et al. (1997)

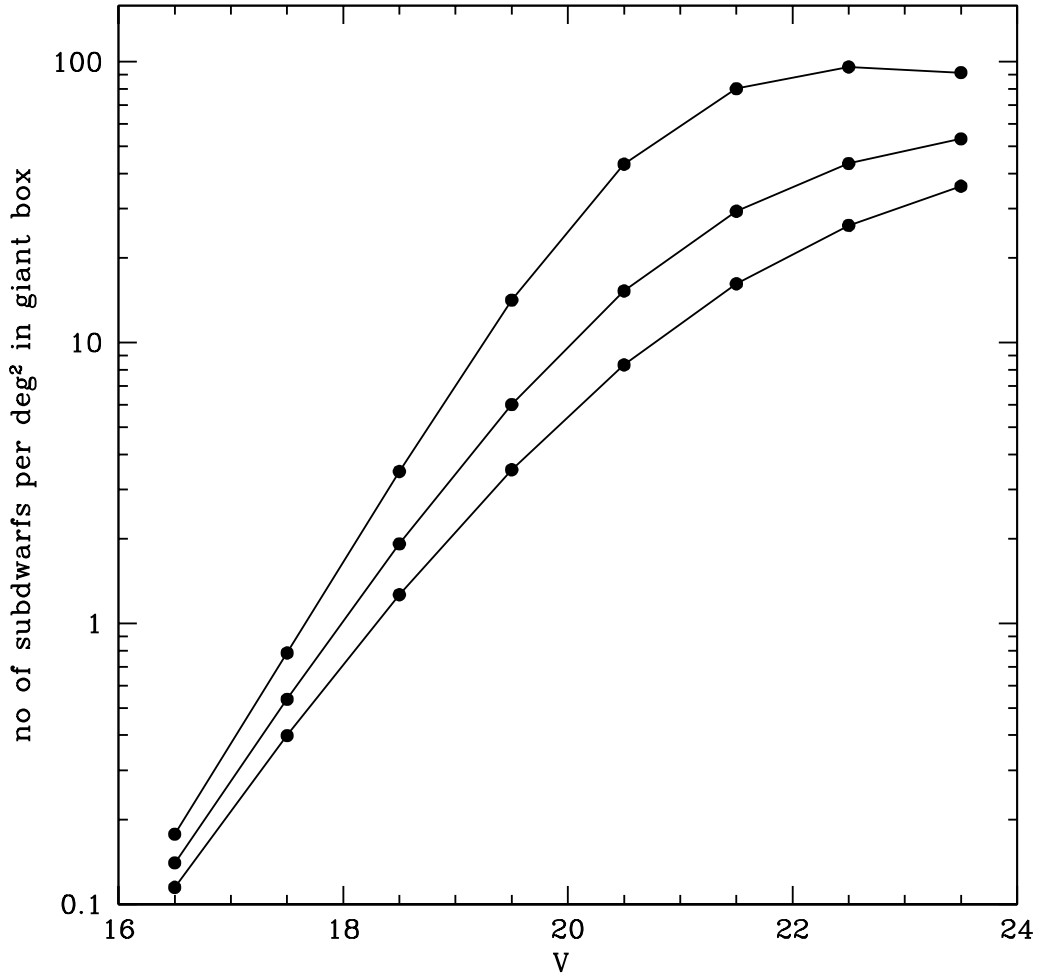


Fig. 2.— Predicted numbers of subdwarfs per unit magnitude interval that will appear in our giant region of the $M-T_2$ vs. $M-51$ diagram. Top line is for $(l, b)=(0, 45)$, middle line for $(l, b)=(90, 45)$ and bottom line for $(l, b)=(180, 45)$. There is less dependence on galactic latitude than longitude, as the r^{-3} density law of the halo contributes most strongly to the increase in counts in fields towards the galactic center.

reach no higher than $M-51=0.05$, corresponding to the value that a blackbody spectrum would have. Thus, apart from photometric errors, we would not expect to see any normal or metal-poor stars with $M-51 > 0.05$. The only other possibility is a spectrum which has *less* light, on average, in the wider M band than in the narrow 51 band close to its center. This can happen if absorption lines in a galaxy’s spectrum are redshifted into the M band, or if an emission line in a galaxy or QSO spectrum is redshifted into the 51 band.

Figure 3 shows the spectrum of a BAL QSO identified in our survey, with the M and 51 filter passbands overlaid⁵. The QSO spectrum is, to first order, featureless over the M passband, although part of the broad emission line at the blue end of the 51 passband would have been included in this filter’s observations, giving the same or slightly more light per Å in the 51 filter than the wider M band.

In addition, the Washington colors of some normal galaxies are similar to those of metal-poor stars, so we will find a small number of galaxies in other regions of the $M-T_2$ vs. $M-51$ diagram. Our survey uses data from mosaic CCD cameras (the Big Throughput Camera and the NOAO mosaics) on the KPNO and CTIO 4m telescopes and the Burrell Schmidt. We are particularly vulnerable to contamination by galaxies in our Schmidt data, where the large pixels make it more difficult to distinguish between stars and galaxies. There is still a small chance of contamination by compact galaxies and QSOs even in our better-sampled BTC and mosaic data. We discuss this further in Section 4.

3. Photometric Errors

Use of the $M-51$ index for luminosity classification requires accurate colors for two reasons. First, the separation between giants and dwarfs in the $M-51$ vs. $M-T_2$ plot is not large: ~ 0.15 mag between solar abundance dwarfs and giants for $M-T_2 > 1.3$ ($B-V > 1.0$) and less for bluer stars. Although metal-poor giants lie further away from the dwarf locus because of their weak Mg b lines, this advantage is offset by the fact that as we move to fainter magnitudes, foreground dwarfs become dominated by thick disk stars, whose lower metallicity ([Fe/H] ~ -0.5 , Carney, Latham and Laird (1989)) moves them toward the giant region. Second, distant giants are strongly outnumbered by foreground disk stars, so we need to cope with the effect of 2σ and even 3σ errors on the dwarf colors.

We use the accurate Washington photometry obtained with the Big Throughput Camera (BTC) on the CTIO 4m telescope in April 1999 (Dohm-Palmer et al. 2000) to illustrate the effect of photometric errors on giant/dwarf classification. This pencil-beam data covers 12.7 square degrees, with latitude ranging from $b = 25$ to 72. For $V < 19$, the median error in $M-T_2$ was 0.012 mag,

⁵the 51 filter passband should be shifted a few Å to the blue to compensate for the fast beam of the CTIO 4m prime focus.

and for $M-51$, 0.013 mag.

We chose a subset of these data with low errors using a magnitude range of $V = 17 - 18.5$ and a maximum error of 0.02 mag in both $M-T_2$ and $M-51$. This subset will be used as an approximation of “zero-error” data which will then be degraded with successively larger photometric errors by adding a number chosen from a gaussian error distribution. The left-hand panel of Figure 4 shows these data, with the regions used by our collaboration and Majewski et al. (2000b)(MOKP hereafter) for giant selection marked. Our giant region is significantly smaller and does not extend as far blueward as the MOKP region. It can be seen that the most numerous stars in this color range have $M-T_2$ between 0.7 and 1.2 ($B-V \sim 0.5-0.9$). These stars are mostly disk dwarfs (Bahcall and Soniera 1984).

We simulated photometric errors by adding gaussian⁶ errors to the observed colors in this low-error subset. The color error in $M-51$ and in $M-T_2$ was chosen randomly from a gaussian distribution with either $\sigma = 0.05$ (middle panel) and 0.10 (right-hand panel) mags. It can be seen that even 0.05 mag color errors move stars into both “giant” boxes, in particular into the region of the MOKP box with $M-T_2 < 1.0$. Color errors of 0.10 mag produce large numbers of bogus giants.

3.1. Where Do the Stars Go?

To quantify the effect of photometric errors on our giant classifications, we need to explore two effects: genuine giants removed from the giant region, and dwarfs and other stars scattered into the giant region by color errors.

The first effect is simpler to quantify because it does not depend on the position in the Galaxy of the field surveyed. Figure 5 illustrates the movement of genuine giants in the $M-51/M-T_2$ diagram for the two classification schemes, assuming that each color was degraded by an amount drawn from a Gaussian with $\sigma = 0.05$ mag. Our smaller giant region leads to a higher loss rate of giants from the box. Figure 6 summarizes the percentage of giants lost due to errors, as a function of the color error. It can be seen that even for color errors as low as 0.02 mag, around 20% of genuine giants will be lost. The most numerous (and least luminous) giant stars lie close to the blue boundary of our giant box at $M-T_2 = 1.1$, and the majority of stars will be lost from this region. This effect, and its dependence on color and absolute magnitude, will need to be taken into account when using halo giants found with $M-51$ to measure the density distribution of the outer halo.

The leakage of foreground dwarfs into the giant regions is more complex to quantify, as it

⁶Often in astronomical datasets we do not have detailed information on the error distribution shape. In general, an error distribution with larger wings will produce more bogus giants, and a distribution with smaller wings than a gaussian will have less effect.

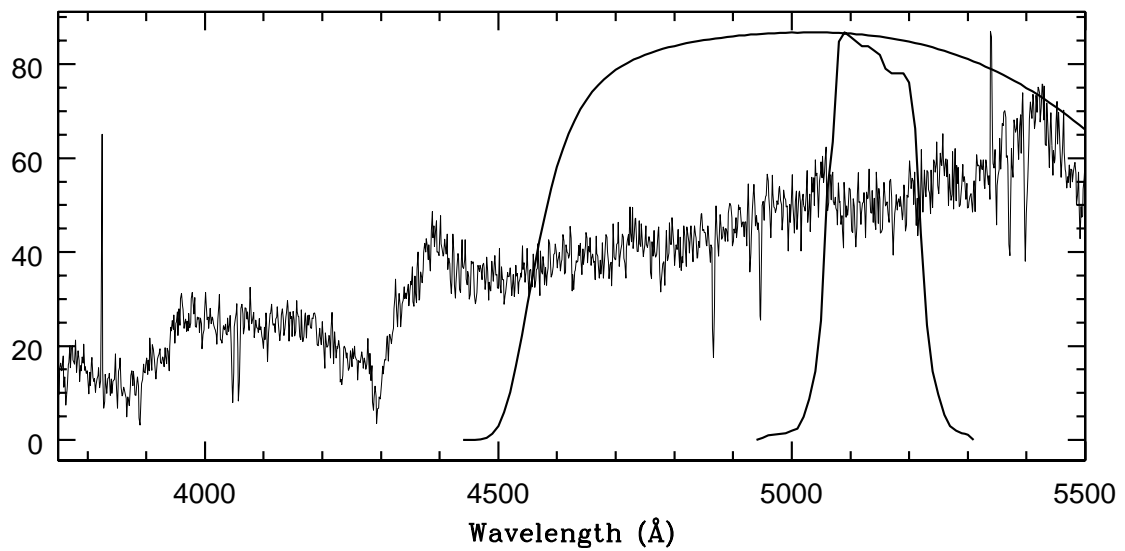


Fig. 3.— Spectrum of BAL QSO at RA=9:16:16.97 Dec=12:16:09.6 (2000), with the M and narrower 51 passbands overlaid. The QSO's relatively featureless spectrum across the M passband, and the broad emission line at the blue end of the 51 band, contribute to its position in the giant box of the $M-T_2/M-51$ diagram.

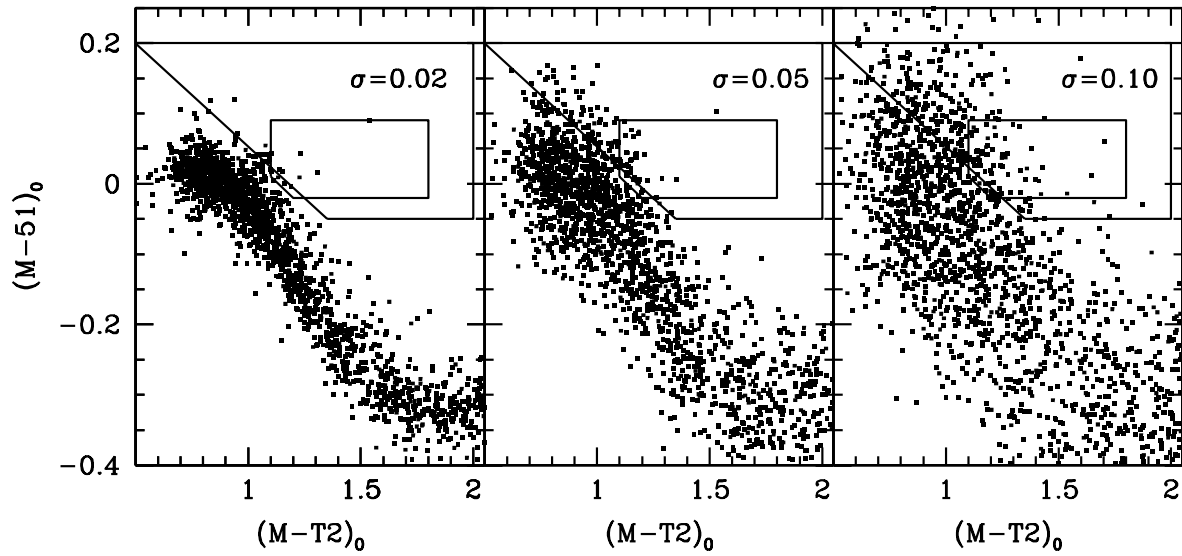


Fig. 4.— $M-T_2$ vs $M-51$ diagrams for BTC data degraded with increasing color errors from left to right. Left-hand panel shows the original data, which has a clearly delineated region occupied mostly by foreground disk stars, middle panel shows the same data with 5% color errors in both $M-T_2$ and $M-51$, right-hand panel show the data with 10% color errors in both filters. The boxes used for giant classification by our collaboration and by MOKP are marked – the MOKP box is larger and stretches significantly bluer.

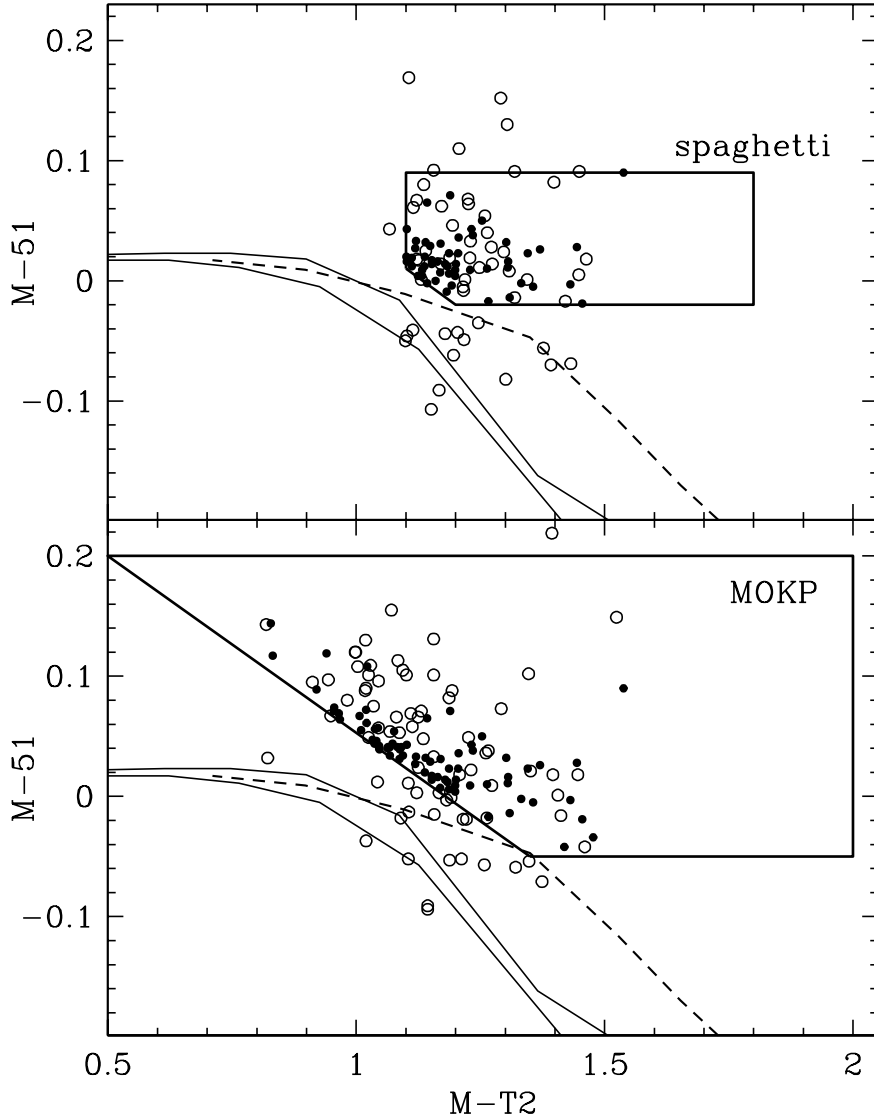


Fig. 5.— For each classification scheme, the movement of stars originally classified as giants in that scheme is shown. Solid circles are original photometry, open circles show these data degraded with a 0.05 mag gaussian error. The box in the top panel shows our (“spaghetti”) classification scheme, with solid lines showing dwarf loci from Paltoglou and Bell (1994) with $[Fe/H] = 0.0$ and -1.0 , and dashed line the solar abundance giant locus from the same paper. The box in the bottom panel shows the classification scheme of MOKP, with the same symbols. It can be seen that more stars are lost out of our giant box because it is smaller.

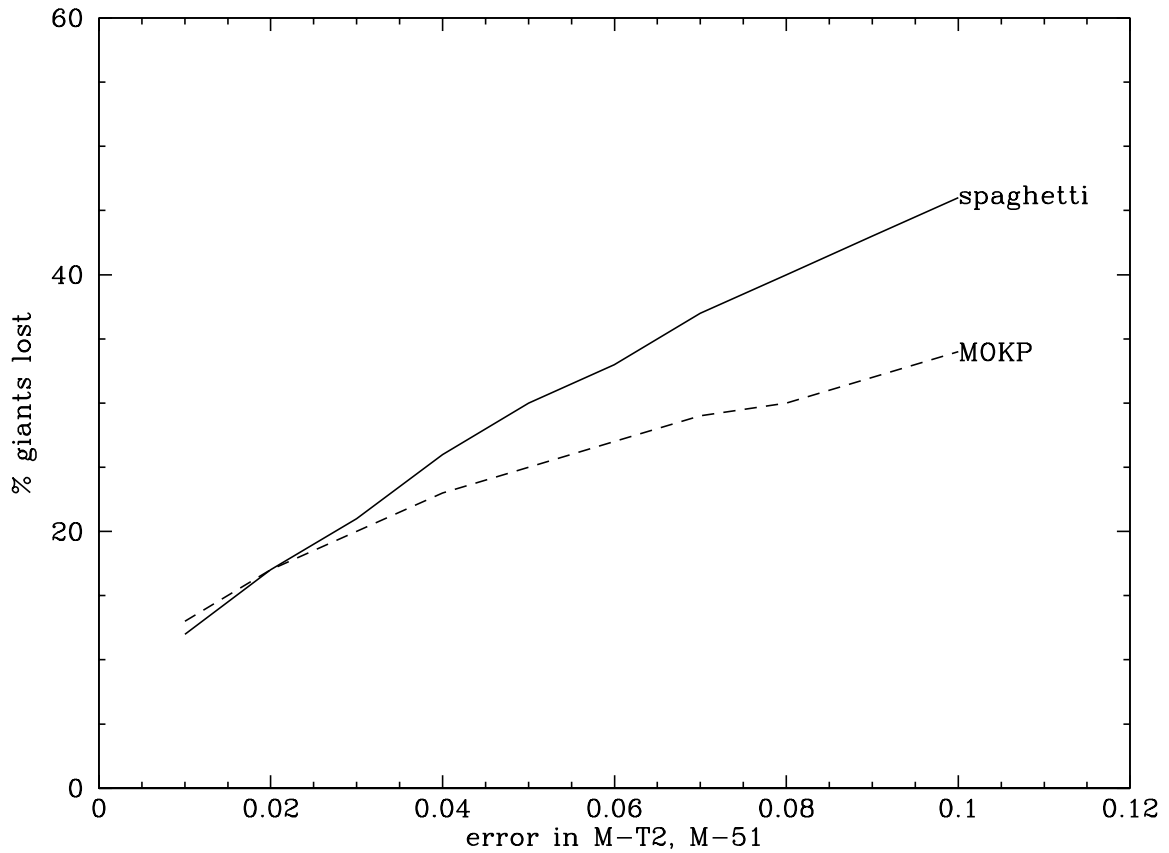


Fig. 6.— Percentage of genuine giants lost due to photometric errors, for our (“spaghetti”) and the MOKP classification schemes. The MOKP scheme loses less giants because of its larger giant classification box.

depends on the numbers of dwarfs close to the boundaries of the giant box. This is a strong function of galactic latitude in particular, since the path length of lower-latitude lines of sight through the disk is higher. Figure 7 illustrates the regions of the color-color diagram where bogus giants originate for both classification schemes, in the case of 0.05 mag errors. (Only stars that will be observed in the faint selection regions will be followed.) For our classification scheme, most of the interlopers are dwarf stars with $M - T_2 = 1.0 - 1.3$ ($B - V = 0.7 - 1.0$). For the MOKP scheme, many more stars are scattered into the giant region. In particular, the blue extension for $M - 51 > 0$ causes problems. The vast majority of stars that find their way into the giant region have $M - T_2 < 1.0$. For stars this blue, the $M - 51$ index has little or no sensitivity to luminosity, as the Mg b /MgH lines become weak for dwarfs and giants alike. The convergence of the dwarf and giant sequences can clearly be seen in Figure 7 of Paltoglou and Bell (1994) for $T_1 - T_2 < 0.4$ ($M - T_2 < 1.0$), and Geisler's original (1984) paper does not even show data for $T_1 - T_2 < 0.38$.

Figures 8 and 9 summarize the balance between the number of giants remaining in the giant region and the number of dwarfs moved into the giant region by photometric error, as a function of color error and galactic latitude. For these simulations we used the BTC data without error cuts, in the magnitude range $V=16-19$, which is typically the magnitude range we use to select giants in our survey (as spectroscopic follow-up becomes difficult fainter than $V=19$ on 4m-class telescopes). The absence of error cuts is because we need to measure how many dwarf stars are in the correct color and magnitude ranges to be moved into the giant region via photometric errors, and limiting the data selected via our errors will lead to incompleteness in our sample. (Note that at these magnitudes the BTC data are essentially 100% complete.) We define a star as a dwarf if it is below the solar abundance giant line in the $M - T_2$ vs. $M - 51$ diagram or if it is bluer than $M - T_2 = 1.0$. This latter requirement will include some blue giants, but the $M - 51$ color holds no information about luminosity this blue. In order to give a feeling for how important this is with respect to the actual numbers of halo giants likely to be found (in a smooth halo) we have used the predictions of the halo model of Morrison (1993) for each latitude bin, and the same magnitude range. (These predictions agree in general with the numbers of halo giants that we have found in our survey fields.) The number of halo giants falls as the error increases because more giants get scattered out of the halo region.

It can be seen from the plots that, especially for low latitudes, large numbers of dwarfs are scattered into the giant box. For our classification scheme, the 50% success point where the number of dwarfs scattered in equals the number of giants not scattered out of the giant box occurs for color errors between 0.035 and 0.045 mag. For the larger giant box of MOKP, the effect is extreme – bogus giants outnumber genuine ones for color errors greater than 0.02 mag. The number of giant candidates that are actually dwarfs can reach more than 100 per square degree for large errors and lower latitudes. It is clear that spectroscopic follow-up of every giant candidate to confirm its luminosity is vitally important. Without it, spurious conclusions will surely result.

With this background behind us, we now consider implications for our own survey and that of MOPKJG.

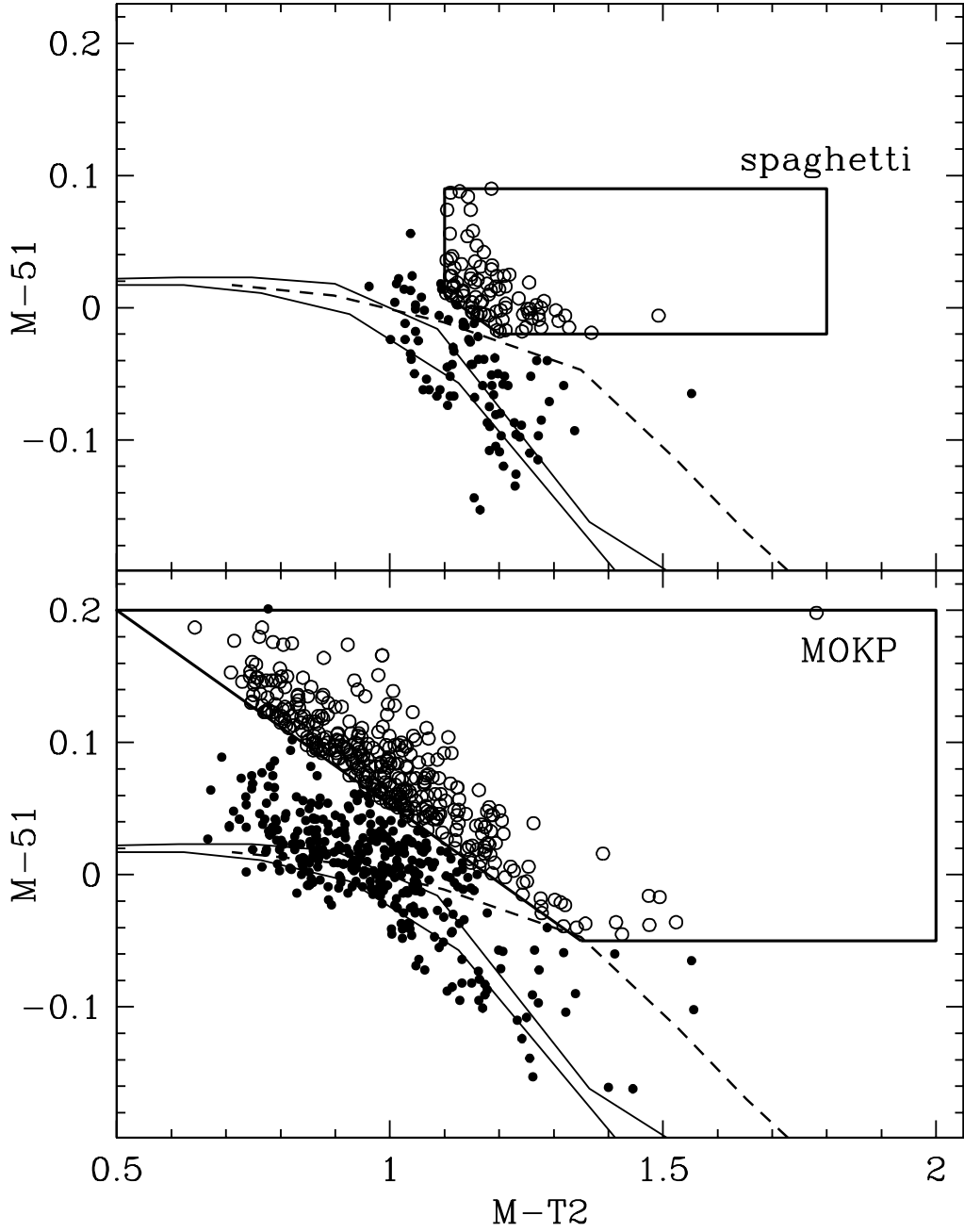


Fig. 7.— Regions where bogus giants, wrongly classified because of their photometric errors, originate for (top panel) our classification scheme and (bottom panel) that of MOKP. Solid symbols denote original colors, open symbols the corresponding point when colors are degraded with a 0.05 mag error drawn from a gaussian distribution. The giant classification box is outlined by a thick solid line in each panel. Thin solid lines show the solar abundance and $[Fe/H]=-1.0$ dwarf loci from the synthetic spectra of Paltoglou and Bell (1994) and the dashed line the solar abundance giant locus from the same work.

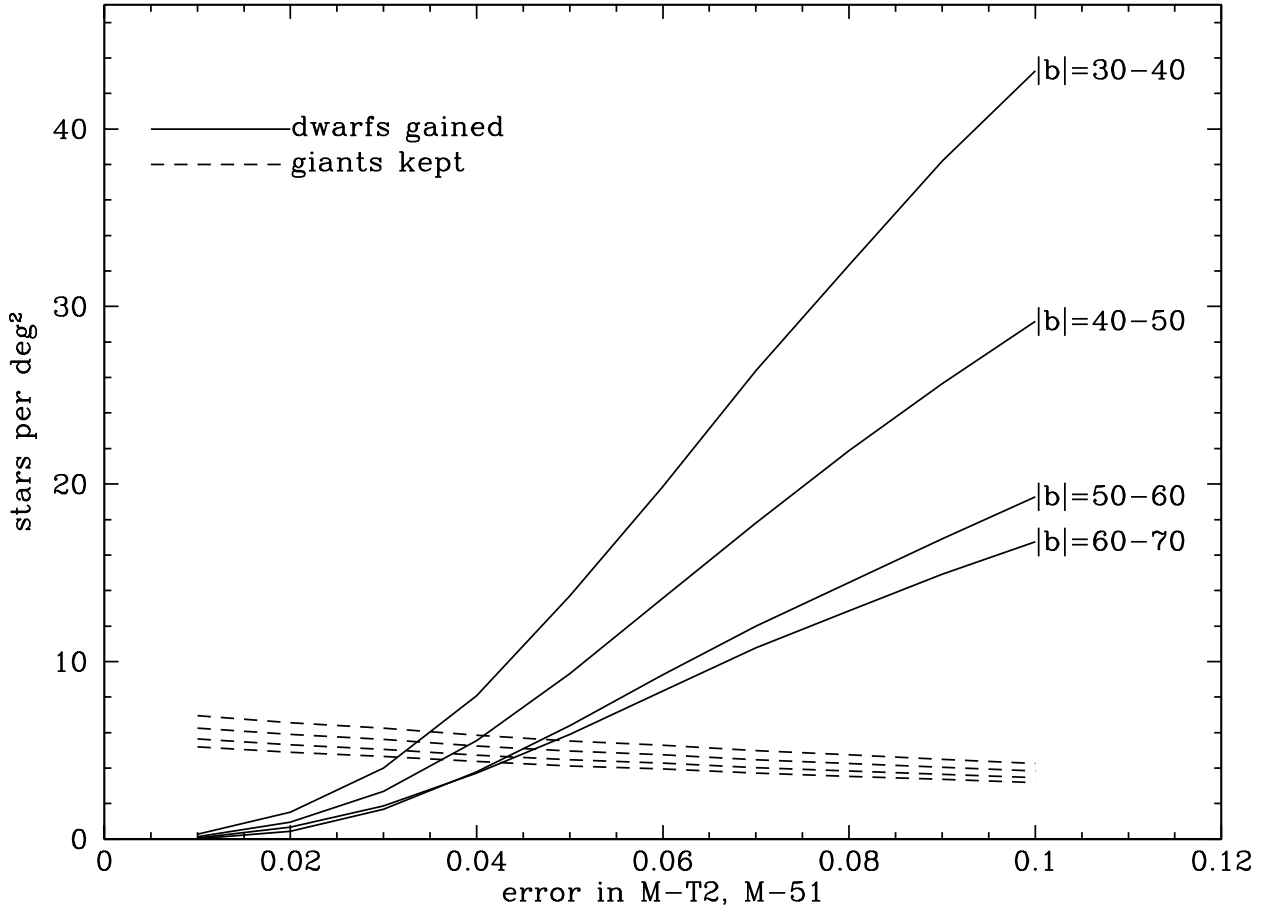


Fig. 8.— The tradeoff between losing giants and gaining dwarfs via photometric errors, for our giant classification region. The BTC data for $16 < V < 19$ were divided into ranges of latitude and both giant and dwarf loss/gain lines were plotted separately for each latitude bin. The giant lines are not labelled for space reasons, but the lowest latitude is denoted by the upper dashed line and the highest latitude by the lowest of the four dashed lines.

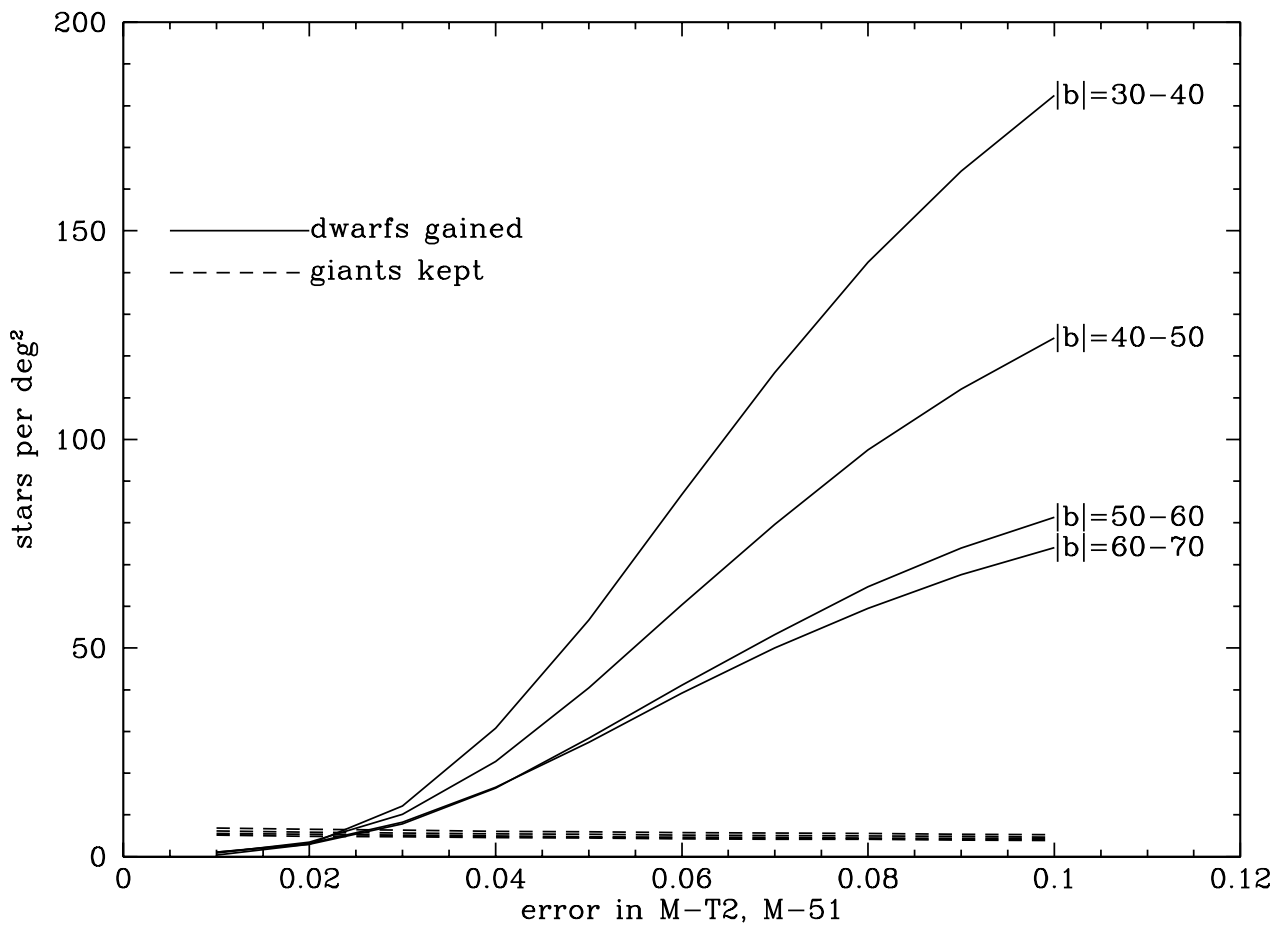


Fig. 9.— Same as Fig. 8 but for the MOKP giant selection scheme. Note the change in scale from Fig. 8.

4. Example 1. Spectroscopic Followup of our BTC Data

Here we describe our spectroscopic follow-up of the BTC imaging data of 12.7 square degrees (Dohm-Palmer et al. 2000), focussing on the dwarfs and other contaminants that we identified. In a future paper (Morrison et al. 2000b) we will describe our spectroscopic calibrations to measure luminosity and metallicity in detail. In three observing runs on the KPNO 4m telescope (in May 1999, January 2000 and March 2000) we observed and classified 57 halo giant candidates, with V magnitudes ranging from $V_0 = 15.6 - 19.2$. This constitutes approximately 50% of our giant candidates in the BTC data.

One candidate (with $V_0=18.7$) was a QSO; so far we have found no galaxies in our BTC data, due to the good spatial sampling of the BTC CCDs.

4.1. Foreground Dwarfs

We have estimated the metallicity of the foreground dwarfs that we identified, by comparing their Mg b /MgH line strength at the observed $M - T_2$ color with that of the dwarf and subdwarf standards observed on these runs (see Table 1 above and Table 2 of Morrison et al. (2000a)). This allowed us to classify them into subdwarfs with $[\text{Fe}/\text{H}] < -2.0$ or metal-richer dwarfs and subdwarfs. Figure 8 of Dohm-Palmer et al. (2000) shows their position in the $M - T_2$ vs. $M - 51$ diagram. Most of the foreground stars that we identified were metal-poor subdwarfs, confirming the efficacy of our luminosity discrimination using accurate $M - T_2$ and $M - 51$ colors. Five stars out of the 57 were classified as dwarfs with $[\text{Fe}/\text{H}]$ greater than -2.0 : two of these were observed before we fully understood the strong effect of errors in scattering dwarfs into our giant box. Since these two stars have errors in both $M - T_2$ and $M - 51$ of 0.04–0.05 mag, it is not unexpected in the light of Section 3 above that they are foreground dwarfs. The other three dwarf stars have low errors and $V_0 > 18$, and this is consistent with the results of Figure 8: even with errors of 0.02 mag in both colors (a little higher than our mean errors at this magnitude), approximately one dwarf per square degree will be scattered into our giant region. (We have observed approximately six square degrees spectroscopically in this field.)

4.2. Extreme Subdwarfs

Out of the 57 halo giant candidates observed, 22 were subdwarfs. (Our giant selection criteria have evolved as we learned more about metal-poor subdwarfs, so some of these stars have colors which place them outside our giant selection box.) Figure 10 shows the histogram of V magnitudes of the 57 halo candidates observed, with the histogram of subdwarf magnitudes overlaid. The magnitude distribution of halo candidates observed reflects the weather and seeing during our 4m spectroscopic runs, rather than the true distribution of halo giants. The sample size is small, but

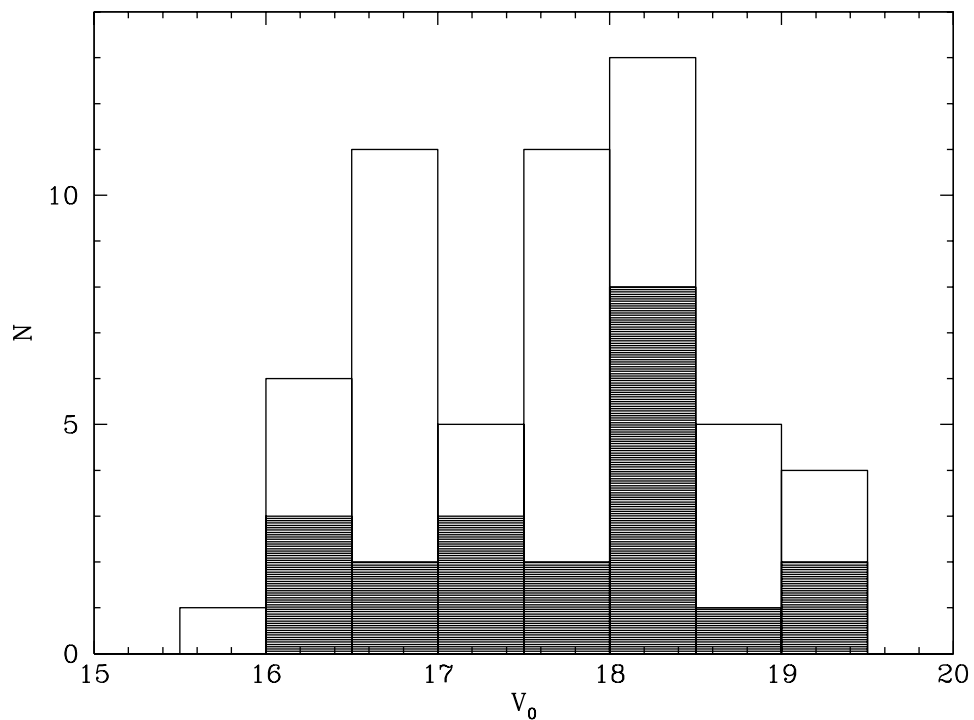


Fig. 10.— Magnitude distribution of the halo giant candidates for which we obtained follow-up spectra, with the histogram of magnitudes of the subdwarf stars shown shaded.

it is still possible to see that the proportion of subdwarfs increases as we go to fainter magnitudes.

Figure 11 shows some examples of spectra of subdwarf stars identified in our BTC survey. Photometry and coordinates for these stars is given in Table 2. Spectral features similar to those of the subdwarf standards shown in Figure 1 are clearly seen: a weak MgH feature and strong CaI 4227 line.

Star l354.18b+66.32 in the middle panel of Figure 11 is a particularly interesting one. Its color and spectrum are similar to that of the subdwarf standard G251-53, with $[\text{Fe}/\text{H}] = -1.9$. The synthetic colors of Paltoglou and Bell (1994) predict that this star should have an $M - 51$ color several hundredths of a magnitude lower than the bottom of our giant selection box, and its $M - 51$ value (-0.041) confirms this prediction. This adds confidence that the estimate of the luminosity function for halo subdwarfs found in our giant box in the Appendix, based on the synthetic colors of Paltoglou and Bell (1994), should be reasonably accurate.

We can make a more direct test of the accuracy of our subdwarf luminosity function by comparing its predictions of the numbers of subdwarfs we should find in our BTC data with the actual number found. Now we restrict consideration to halo giant candidates *inside* our giant selection box with photometric $[\text{Fe}/\text{H}]$ estimate less than -1.0 , and limit the magnitude range to $V_0 < 19.0$. Of the 53 BTC fields, 14 have complete spectroscopic follow-up of giant candidates, and 8 subdwarfs were identified. Another 13 fields have no giant candidates at all. Assigning the correct percentage of “no giant candidate” fields to the spectroscopic follow-up group, we find that 4.45 square degrees have been completely surveyed for giants. This gives a subdwarf frequency of 1.8 ± 0.6 per square degree. The fields with complete spectroscopic follow-up have a mean $(l, b) = (281, 47)$, so the middle line in Figure 2 is a good match. This predicts 2.6 subdwarfs per square degree in our giant selection box down to $V=19$, in good agreement with our actual value, once errors in the local halo density are taken into account.

In summary, our spectroscopic follow-up has confirmed the importance of accurate photometry for giant selection using the Washington system. In addition, the number of subdwarfs found in our fields is in agreement with the predictions of the model described in Section 2.2.1 and the Appendix. Particularly for V magnitudes fainter than 18, *photometric identification of halo giants*

Table 2. Photometry for subdwarf stars in Fig. 11

Star ID	RA	Dec	epoch	M_0	$(M - T_2)_0$	$M - T_2$ error	$(M - 51)_0$	$M - 51$ error
l272.01b+69.46	12:09:20.85	9:09:08.6	2000	17.625	1.383	0.009	-0.093	0.009
l293.26b+71.69	12:39:11.00	9:03:07.5	2000	18.718	1.356	0.011	-0.004	0.010
l354.18b+66.32	14:05:55.81	11:10:29.1	2000	18.702	1.420	0.009	-0.042	0.016
l233.99b+31.77	9:21:16.95	-1:49:28.8	2000	19.183	1.140	0.010	0.004	0.011
l237.12b+58.44	10:54:50.52	11:24:06.4	2000	18.225	1.148	0.011	0.018	0.011

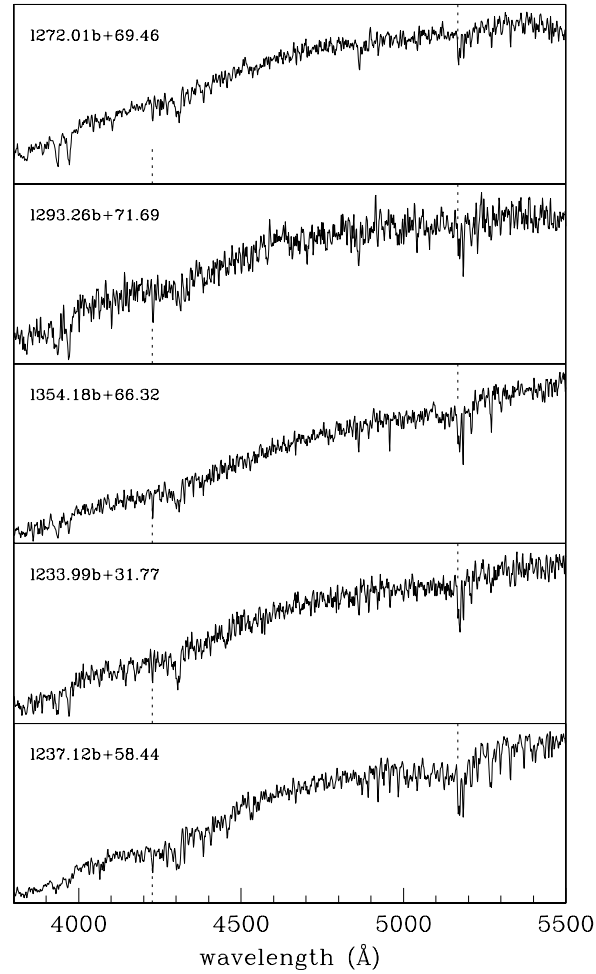


Fig. 11.— Spectra of subdwarf stars identified in our halo survey. Positions of the Ca I 4227Å line and the Mg 5167Å line are marked.

is not enough: spectroscopic confirmation of their luminosity is very important.

4.3. Efficiently Selecting Faint Giants

If we observe every giant candidate that appears in the giant region of Figure 15 (see Appendix) spectroscopically for V fainter than 18, we will find three subdwarfs for every genuine halo giant. The stars that are of particular interest in this magnitude range are the high-luminosity giants which help trace the extreme outer halo, like our star l304.49b+60.51 (Olszewski et al. 2000). With accurate photometry, it is possible to make our spectroscopic follow-up more efficient by utilizing the sensitivity of the $M-51$ color to luminosity.

Figure 12 shows the halo giants and subdwarfs identified by spectroscopic follow-up, with giants coded by absolute magnitude. It can be seen that the most luminous giants are not only the reddest, but also occupy the upper region of the giant box, with $M-51 > 0.01$, while the subdwarfs cluster toward the bottom left.

For our survey, if we restrict our giant selection box to the upper right of the original region for $V > 18$, we are able to optimize our efficiency of giant selection without missing any of the most distant giants in our sample. For data that reach fainter levels, this "new, clean" region becomes contaminated with intrinsically fainter, redder subdwarfs.

5. Example 2. The MOPKJG Survey of the Carina Dwarf Spheroidal Galaxy

Majewski et al. (2000a) present Washington M , T_2 , 51 photometry of a field of area $\sim 2 \text{ deg}^2$ centered on the Carina dwarf spheroidal galaxy, and use both the $M-T_2$ vs. $M-51$ diagram and the locus of the Carina red giant branch in the M_0 vs. $M-T_2$ diagram to identify a large number (~ 100) of Carina-associated giant candidates *outside* the tidal radius of Irwin and Hatzidimitriou (1995). These stars range in magnitude from $M_0=17.8-20.8$ ($V \simeq 17.5-20.5$). They obtained confirmatory spectroscopy of three of the brightest extratidal giant candidates, which are 1.4σ , 1.4σ and 2.3σ outside the Irwin and Hatzidimitriou (1995) tidal radius, using their quoted error of 3.6 arcmin. Based on the number of extratidal giant candidates, they derive a surprisingly high mass-loss rate: 27% of the total mass of Carina per Gyr.

Because their survey covers a relatively small area, contamination by subdwarfs in their giant region is not a significant problem. We make a conservative estimate of the number of subdwarfs in their giant region by using the luminosity function derived in the Appendix for our smaller giant region: the halo model predicts that 14 subdwarfs will be found per square degree to $V=20.5$ ($M \simeq 20.8$).

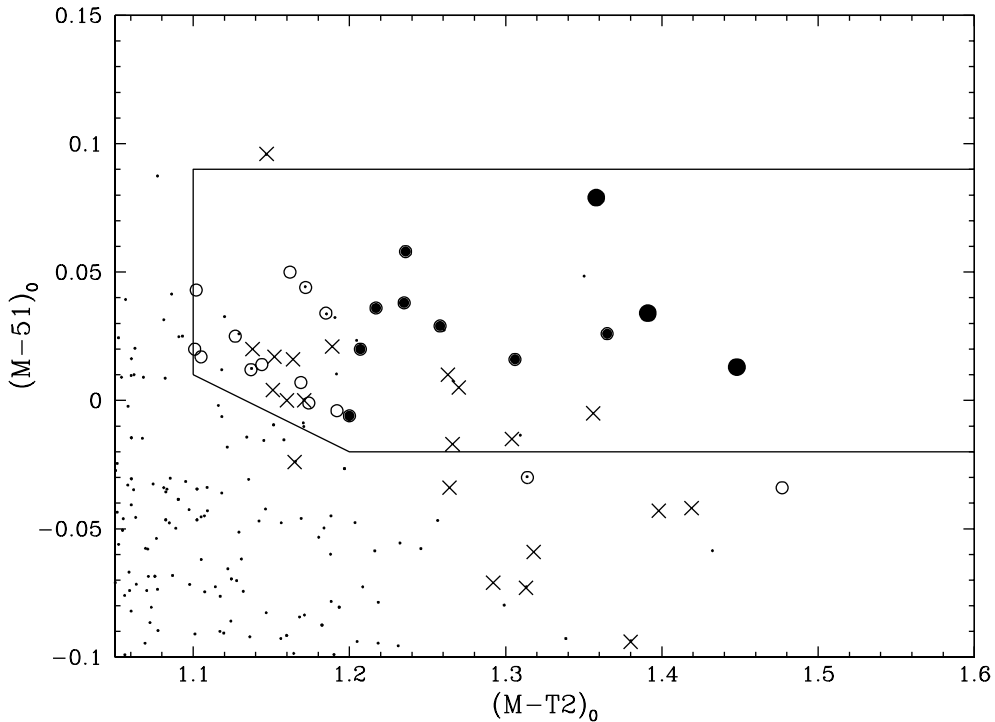


Fig. 12.— Position of our most luminous giants in the $M - 51$ vs. $M - T_2$ diagram. Our giant selection box is outlined, and the small dots represent the photometry from a subsample of our survey fields to show the locus of foreground stars. Subdwarfs are shown as crosses and giants as circles. Open circles are the least luminous giants, with $M_V > 0.5$, small closed circles are giants with $-0.5 < M_V < 0.5$, large closed circles are giants with $M_V < -0.5$. The most luminous giants are in the upper right region of our giant box while the subdwarfs occupy the bottom left for this magnitude range.

5.1. Effect of Photometric Errors

Carina has quite a low galactic latitude ($b = 22$) so there are large numbers of disk stars in the foreground, and the potential exists for a significant number to scatter into the giant region of the $M - T_2/M - 51$ diagram. The accuracy of the Majewski et al. (2000a) photometry is not high. This is caused in great part by their short exposure times: their C40 telescope exposure times in M and T_2 were almost the same as our 4m BTC exposure times, 15 times shorter when the difference in aperture is taken into account. (Their 51 exposures were a factor of ~ 3 shorter after correcting for telescope aperture.) MOPKJG work more than a magnitude fainter than our survey, to $M = 20.8$ ($V \simeq 20.5$). In addition, the C100 data suffered from such large PSF variations that even a quadratic variable PSF in DAOphot was unable to completely correct them.

To deal with these large errors they restrict consideration to stars with errors in all filters less than 0.10 mag. Thus it is possible for stars with color errors as high as 0.14 mag in $M - 51$ or $M - T_2$ to be included in their sample. In Figure 9 we showed that at latitudes of 30–40 degrees, significantly higher than the latitude of Carina, almost 200 dwarf stars per square degree are scattered into the MOKP giant box for color errors of 0.10 mag. Thus the additional cut using the Carina giant branch is very important.

MOPKJG estimate the contribution of “background” objects by successively displacing the Carina giant branch region to *brighter* magnitudes, and counting how many stars which satisfy their $M - 51/M - T_2$ cut are found in the shifted giant branch region. Their decision to only shift the box to brighter magnitudes is forced upon them by the serious incompleteness of their photometry at magnitudes fainter than $M=20.8$. This is unfortunate, because the number of interlopers in the giant region increases sharply at fainter magnitudes, so their background estimates will be systematically too small.

The magnitude range of interest for Carina giants is $M_0=17.8$ –20.8. Here, the majority of the C100 photometry has errors ranging up to 0.15 mag in M and 51 and 0.25 mag in T_2 . The C40 data has larger errors: up to 0.40 mag in 51, 0.25 mag in T_2 and 0.3 mag in M . With an error cut of 0.10 mag per filter and a significant number of stars having errors in each filter close to this number, color errors of up to 0.14 mag are likely. We have extended our simulations of the likely number of foreground dwarfs that will be moved into the MOKP giant selection box in the $M - 51/M - T_2$ diagram by adding the same selection as was used by MOPKJG (the CMD bounding box outlined in their Figure 8) to isolate stars at the right color and magnitude to be on Carina’s giant branch. Figure 13 shows our results. It can be seen that with color errors in the range of 0.05 to 0.10 mag, dwarf contamination is significantly higher than that claimed by MOPKJG, whose largest extratidal background estimate was 22 stars per square degree. Even the extra cut using the position of Carina’s red giant branch would not rid the extratidal giant sample of many interlopers.

In summary, more spectroscopic follow-up is needed to confirm the claim of Majewski et al. (2000a) that Carina is losing 27% of its mass per Gyr. With photometric errors of 0.10 mag, the typical star in the giant region will be a photometric error. Brighter stars, such as the three

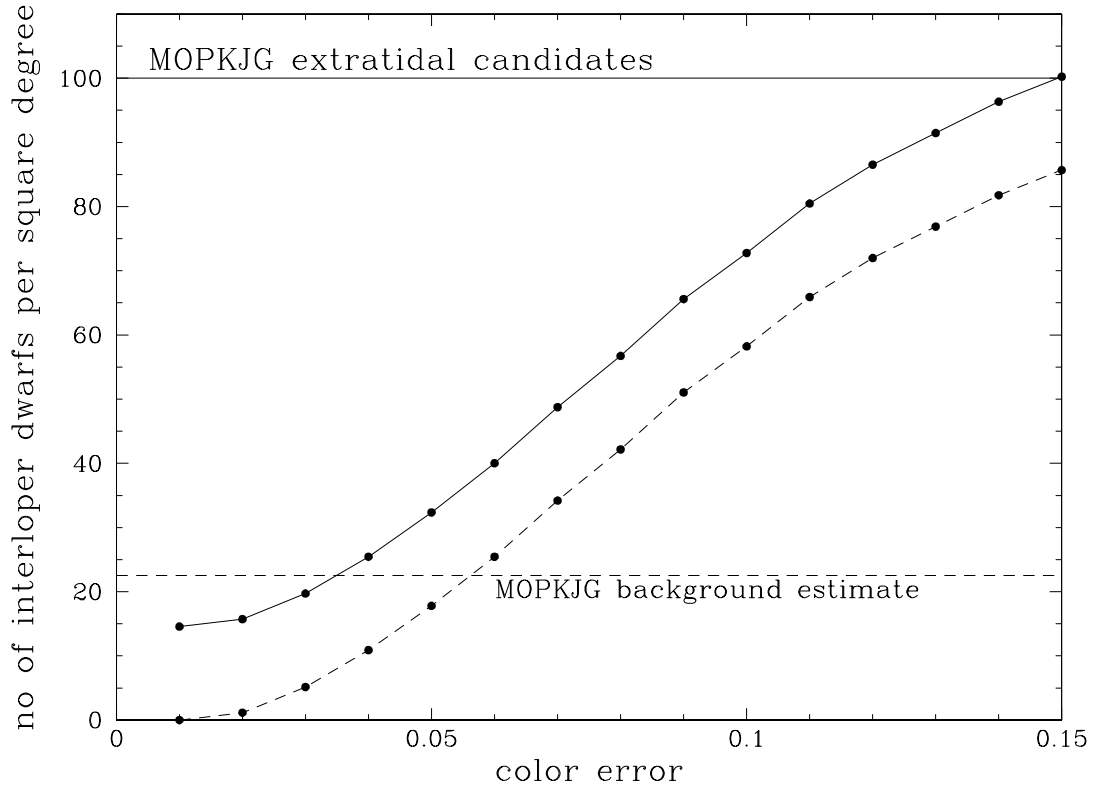


Fig. 13.— Our prediction of number of foreground dwarfs (dashed curve) and foreground dwarfs including metal-poor subdwarfs (solid curve) that will be scattered into the MOPKJG giant selection regions in the $M-T_2/M-51$ and $M-T_2/M$ diagrams, as a function of photometric error, for M magnitudes brighter than 20.8. MOPKJG’s estimated background level and number of extratidal giants per square degree are also shown with straight lines, dashed and solid respectively.

observed spectroscopically, will have smaller photometric errors and will in general be giants if they are in the giant region. However, only one of these is more than 2σ away from the Irwin and Hatzidimitriou (1995) tidal radius. A larger spectroscopic sample is needed. The discovery of one extratidal bright giant tells us nothing about the discovery fraction of fainter giants.

6. Summary

Washington photometry, with the addition of the 51 filter, is a powerful method of finding distant halo giants. We find that at the faintest magnitudes probed by our survey, our giant selection efficiency falls, and we make a careful examination of possible problems with the Washington giant classification to improve future surveys. We show that accurate photometry (color errors less than 0.03 mag) is essential to cut down on the scattering of the numerous foreground dwarfs into the giant region in the $M-51/M-T_2$ color-color plot. We have made estimates of the contamination of giant candidates by very metal-poor halo dwarfs by deriving a new luminosity function specifically for the subdwarfs which mimic halo giants in the $M-51/M-T_2$ diagram, and using it in a simple halo model.

We used our results on luminosity discrimination with the Washington system to examine two recent surveys: our own survey of 12.7 square degrees at high galactic latitudes (Morrison et al. 2000a; Dohm-Palmer et al. 2000), and the study of Majewski et al. (2000a) of fields centered on the Carina dwarf spheroidal galaxy, which finds over 100 Carina-associated giant candidates outside its tidal radius.

For surveys such as our own of the halo field, very metal-poor halo dwarfs are the major source of contamination of candidate giant samples, and we propose using a smaller region of the $M-51/M-T_2$ diagram to optimise spectroscopic follow-up at the faint magnitudes where the subdwarfs dominate. The survey of Majewski et al. (2000a) has spectroscopic follow-up only for three of the brightest “extra-tidal” giant candidates, and we show that their photometric errors, which will increase as stars become fainter, can have a very serious effect on their giant classification.

In summary, spectroscopic follow-up of giant stars identified using the Washington system is vital. If one wishes to make statistical corrections for the number of bogus giants caused by photometric errors, it is important to quantify accurately the photometric errors in the data, both in terms of the size of the average error and the shape of the distribution.

We would like to thank the referee, Bruce Carney, for helpful comments. This work was supported by NSF grants AST 96-19490 to HLM, AST 95-28367, AST96-19632 and AST98-20608 to MM, and AST 96-19524 to EWO.

APPENDIX: Luminosity Function for Halo Dwarfs with $[\text{Fe}/\text{H}] < -2.0$

We have derived a luminosity function (LF) for halo G and K dwarfs with $[\text{Fe}/\text{H}] < -2.0$ using LFs for four metal-poor globular clusters derived from HST WFPC2 color-magnitude diagrams by Piotto, Cool and King (1997), and the splendid $V, V-I$ color-magnitude diagram of NGC6397 of King et al. (1998), transformed to the standard Landolt system using the transformations of Holtzman et al. (1995).

We need to derive a LF separately for the metal-poor stars – its slope will be different for the halo as a whole and for its most metal-poor stars. This can be seen in the compilation of accurate globular cluster LFs of Paresce and De Marchi (2000), where for $M_I=5-8$, clusters such as NGC6397 have relatively more stars at the faint end than metal-richer clusters such as NGC6752 and NGC104. Also, since we are interested in the luminosity distribution at a given color, we need to use the color-magnitude diagram of a metal-poor cluster to decide which absolute magnitudes appear in our $M-T_2$ color range for stars with $[\text{Fe}/\text{H}] < -2.0$, where our ability to discriminate them via $M-51$ begins to fail.

Although it would be more direct to use a subsample of the Bahcall and Casertano (1986) field star data with $[\text{Fe}/\text{H}] < -2.0$ to derive this LF, the Bahcall and Casertano (1986) sample is too small. It is based on only 51 stars in our magnitude range of interest ($M_V=6-9$), and is particularly poorly sampled at the bright end. Thus we use accurate LFs derived from HST photometry of metal-poor globular clusters, where there are sufficient stars to remove concerns about Poisson counting errors. We first compare the LF from a cluster with a similar $[\text{Fe}/\text{H}]$ to the mean of the halo field (Paresce and De Marchi 2000, NGC 6752) with the Bahcall and Casertano (1986) halo field LF to check for cluster-field differences, as halo field stars may not have formed under identical conditions to globular clusters. (The cluster was observed near its half-light radius where mass segregation effects are minimal.) It can be seen in Figure 14 that these two LFs are very similar.

We then proceed to construct our metal-poor halo LF using the clusters M15, M30, M92 and NGC6397 (whose $[\text{Fe}/\text{H}]$ values range from -1.9 to -2.2 , Zinn 1985). Piotto, Cool and King (1997) compare the LFs of their four globular clusters and note that three (M15, M30 and M92) are in good agreement, while the LF of NGC 6397 has fewer stars for $M_V > 7$ than the other clusters. They calculate multi-mass King models in order to check whether corrections are needed to convert their local LFs to global ones, and conclude that any corrections will not exceed one or two tenths in the logarithm. Thus, since Piotto, Cool and King (1997) were unable to relate the only difference in the LF slopes to mass segregation effects, we choose to simply average the four LFs.

Figure 14 shows this LF, compared to that of Bahcall and Casertano (1986) for halo field stars, calculated with a “discovery fraction” of 0.5 (Morrison 1993). The cluster LFs were normalized to agree with the Bahcall and Casertano (1986) LF for $M_V=6-8$. As expected, the metal-poor LF has more stars at the faint end than the Bahcall and Casertano (1986) LF and the NGC 6752 one.

With this luminosity function, it is possible to predict numbers of K dwarfs with $[\text{Fe}/\text{H}] < -2.0$

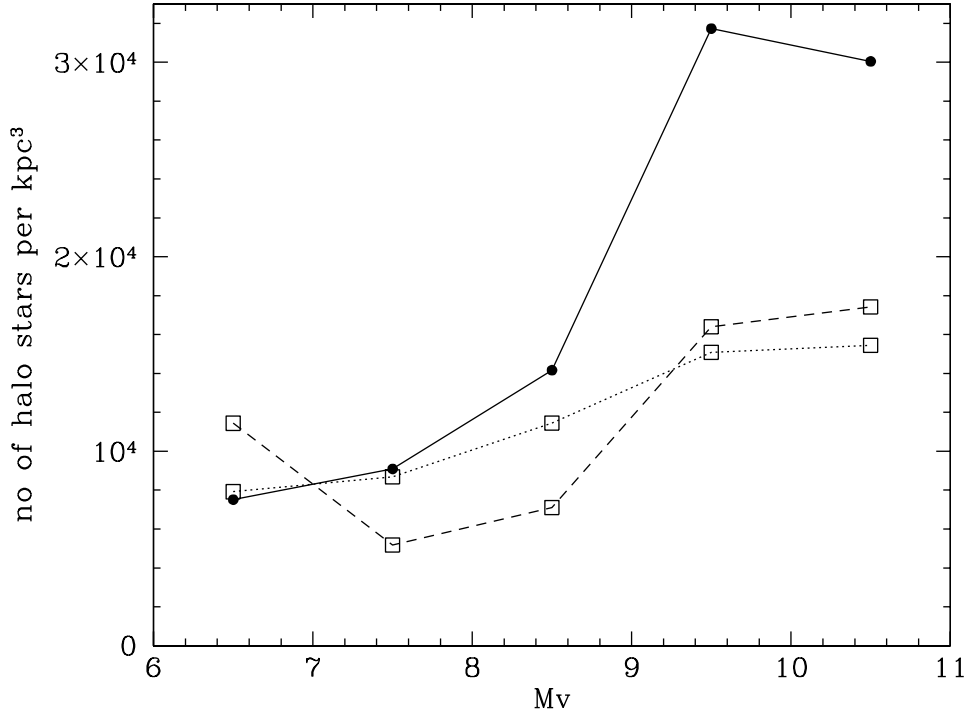


Fig. 14.— Comparison of halo field LF of Bahcall and Casertano (1986) (dashed line) with the average of the accurate LF of NGC 6752 (Paresce and De Marchi 2000, dotted line) and the average of the LFs of four metal-poor globulars from Piotto, Cool and King (1997) (solid line). The cluster LFs were normalized to the field LF for $M_V=6-8$.

in the color range corresponding to our giant box, as a function of magnitude and position in the Galaxy. For relatively bright stars ($V < 19$) we only probe out to distances of 3 kpc at most. As in Paper I, we used the metallicity distribution of Ryan and Norris (1991) to determine that 31% of halo dwarfs have $[\text{Fe}/\text{H}] < -2.0$. The rare subdwarfs with $[\text{Fe}/\text{H}] \leq -3.0$, such as G160-30, are of particular concern to us because it requires higher signal-to-noise in the follow-up spectrum to determine whether the star is a dwarf or giant. We used the metallicity distribution of Beers (1999), which is complete for metallicities below -2.0 , and contains 4754 stars in total, to determine that 3% of all halo dwarfs have $[\text{Fe}/\text{H}] \leq -3.0$. (Within the errors, this is consistent with the result of Ryan and Norris (1991).)

It can be seen in Figure 15, which shows the synthetic colors of Paltoglou and Bell (1994) for dwarfs of different metallicity, that our giant selection box overlaps the $[\text{Fe}/\text{H}] = -2.0$ subdwarfs only at its blue end ($M - T_2 = 1.1 - 1.3$) and overlaps the $[\text{Fe}/\text{H}] = -3.0$ lines for a larger color interval ($M - T_2 = 1.1 - 1.6$). In other words, for the coolest K dwarfs in our color range, the Mg lines are sufficiently strong that only the most metal-poor ($[\text{Fe}/\text{H}] \leq -3.0$) appear in our giant selection box, while for the warmer K dwarfs, the lines are weaker and so stars with $[\text{Fe}/\text{H}] \leq -2.0$ appear in

our giant selection box. We took this into account in the construction of the luminosity function for the halo subdwarf model, by scaling the numbers of dwarfs with bluer colors (brighter absolute magnitudes) by 31% and those with redder colors (fainter absolute magnitudes) by 3%.

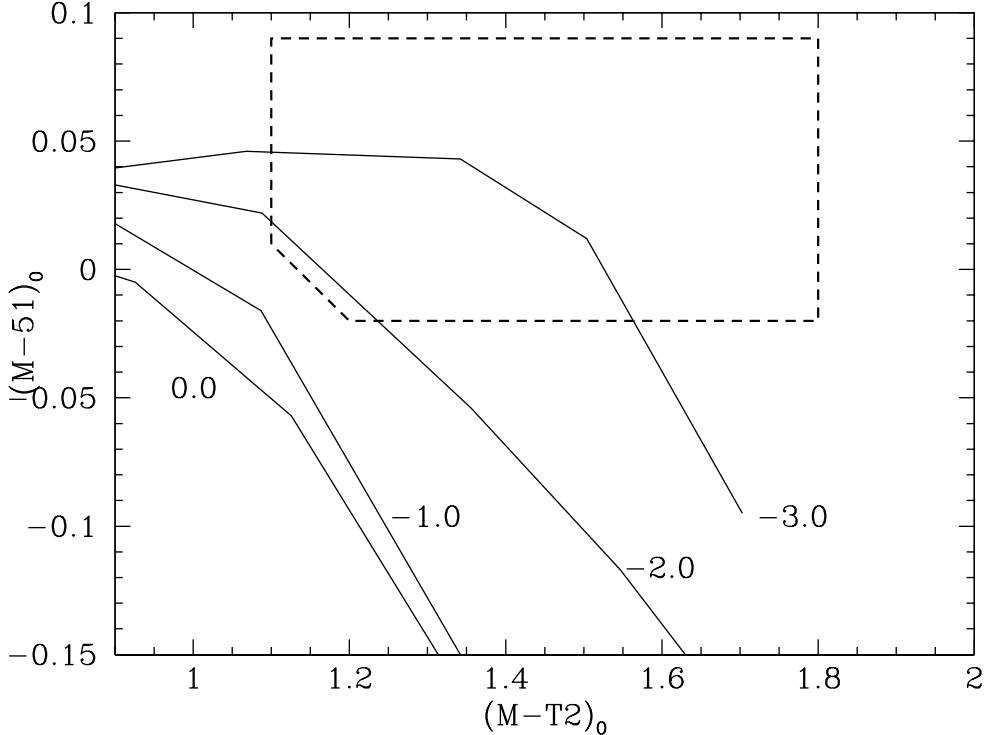


Fig. 15.— This figure illustrates the region of our giant selection box (shown with a dotted line) that overlaps with the synthetic dwarf loci of Paltoglou and Bell (1994) for $[Fe/H] = -2.0$ and -3.0 .

Table 3 gives the luminosity function for metal-poor subdwarfs derived from the clusters in Piotto, Cool and King (1997), and the luminosity function specifically calculated to match the number of metal-poor dwarfs that will appear in our giant box.

REFERENCES

Alexander, D. R., Brocato, E., Cassisi, S., Castellani, V., Ciacio, F. and degl'Innocenti, S. 1997, A&A, 317, 90

Alonso, A., Arribas, S. and Martinez-Roger, C. 1996, A&AS, 117, 227

Bahcall, J.N. & Casertano, S. 1986, ApJ, 308, 347

Bahcall, J. & Soniera, R. 1984, ApJS, 55, 67

Table 3. Luminosity functions for metal-poor dwarfs

M_V range	$M-T_2$ range	Metal-poor LF (stars per kpc^3)	“Giant interloper” LF (stars per kpc^3)
6.0–6.5	0.93–1.05	3245	0
6.5–7.0	1.05–1.17	4268	662
7.0–7.5	1.17–1.30	4073	1262
7.5–8.0	1.30–1.43	5014	150
8.0–8.5	1.43–1.60	6036	181
8.5–9.0	1.60–1.76	8130	0
9.0–9.5	1.76–1.83	15497	0

Beers, T.C., 1999, in The Galactic Halo, ASP Conf. Series Vol 165, eds. B.K. Gibson, T.S. Axlerod and M.E. Putman

Bessell, M.S. 2000, submitted to PASP

Beveridge, R. C. and Sneden, C. 1994, AJ, 108, 285

Bond, H. E. 1980, ApJS, 44, 517

Canterna, R. 1976, AJ, 81, 228

Carbon, D. F., Barbuy, B., Kraft, R. P., Friel, E. D. and Suntzeff, N. B. 1987, PASP, 99, 335

Carney, B. W., Latham, D. W. and Laird, J. B. 1989, AJ, 97, 423

Carney, B.W., Aguilar, L., Laird, J.B. and Latham, D.W. 2000, in preparation.

Dohm-Palmer, R. C., Mateo, M., Olszewski, E. W., Morrison, H. L., Harding, P., Freeman, K. C. and Norris, J. E. 2000, submitted to the Astronomical Journal (Paper II)

Geisler, D. 1984, PASP, 96, 723

Geisler, D., Claria, J.J. & Minniti, D. 1991, AJ, 102, 1836

Geisler, D., Claria, J. J. and Minniti, D. 1997, PASP, 109, 799

Gratton, R. G., Fusi Pecci, F., Carretta, E., Clementini, G., Corsi, C. E. and Lattanzi, M. 1997, ApJ, 491, 749

Harris, H. C. and Canterna, R. 1979, AJ, 84, 1750

Helmi, A. & White, S.D.M. 2000, submitted to MNRAS (astro-ph 0002482)

Holtzman, J. A., Burrows, C. J., Casertano, S., Hester, J. J., Trauger, J. T., Watson, A. M. and Worthey, G. 1995, PASP, 107, 1065

Irwin, M. and Hatzidimitriou, D. 1995, MNRAS, 277, 1354

Ivans, I. I., Carney, B., de Almeida, L. and Sneden, C. 2000, astro-ph 007065, to appear in "Dynamics of Star Clusters and the Milky Way", (eds) S. Deiters, B. Fuchs, A. Just, R. Spurzem and R. Wielen, ASP Conference Series.

King, I. R., Anderson, J., Cool, A. M. and Piotto, G. 1998, ApJ, 492, L37 D.W. 1988, AJ, 95, 1843

Majewski, S. R., Ostheimer, J. C., Kunkel, W. E., Johnston, K. V., Patterson, R. J. and Palma, C. 1999, IAU Symposia, 190, 508

Majewski, S. R., Ostheimer, J. C., Kunkel, W. E. and Patterson, R. J. 2000, astro-ph 006411 (MOKP)

Majewski, S. R., Ostheimer, J. C., Patterson, R. J., Kunkel, W. E., Johnston, K. V. and Geisler, D. 2000, AJ, 119, 760 (MOPKJG)

McClure, R. D. and Forrester, W. T. 1981, Publications of the Dominion Astrophysical Observatory Victoria, 15, 14

McWilliam, A. 1990, ApJS, 74, 1075

Morrison, H.L. 1993, AJ, 106, 578

Morrison, H. L., Mateo, M., Olszewski, E. W., Harding, P., Dohm-Palmer, R. C., Freeman, K. C., Norris, J. E. and Morita, M. 2000, AJ, 119, 2254 (Paper I)

Morrison, H. L., Norris, J.E., Mateo, M., Olszewski, E. W., Harding, P., Dohm-Palmer, R. C. and Freeman, K. C. 2000, in preparation.

Olszewski, E. W., Morrison, H. L., Mateo, M., Harding, P., Dohm-Palmer, R. C. Freeman, K.C. and Norris, J.E. 2000, in preparation.

Paltoglou, G. & Bell, R.A. 1994 MNRAS, 268, 793

Paresce, F. and De Marchi, G. 2000, ApJ, 534, 870

Piotto, G., Cool, A. M. and King, I. R. 1997, AJ, 113, 1345

Ryan, S. G. 1992, AJ, 104, 1144

Ryan, S.G. and Norris, J.E. 1991, AJ, 101, 1835

Schlegel, D.J., Finkbeiner, D.P. & Davis, M. 1998, ApJ, 500, 525

Tomkin, J. and Lambert, D. L. 1999, ApJ, 523, 234

Zaritsky, D., Olszewski, E. W., Schommer, R. A., Peterson, R. C. and Aaronson, M. 1989, ApJ, 345, 759

Zinn, R.J. 1985, ApJ, 293, 424